COLLIMATION SYSTEM DESIGN FOR LCLS-II

M. W. Guetg*, P. J. Emma, M. Santana Leitner, J. J. Welch, F. Zhou,
SLAC National Accelerator Laboratory, Menlo Park, CA 94025, USA

Abstract

The planned LCLS-II FEL has an average beam power of up to 1.2 MW and a repetition rate of up to 1 MHz, both of which entail serious challenges for beam halo collimation. This paper summarizes the efforts to assess the proposed collimation system. The undulator section is specifically focused on due to its high loss sensitivity (maximal 12 mW). This proceedings concentrate on field emissions of the gun. Different dark current distribution, linac configurations and simulation programs were used to increase assurance of the results. Filled phase-space tracking further supplemented an independent prove of the collimation system effectiveness and expands to include beam-halo originating from different sources than the gun.

INTRODUCTION

LCLS-II [1] is a planned upgrade to the LCLS at SLAC. It includes the addition of a high average power superconducting linac with a nominal final electron energy of 4 GeV and a repetition rate of up to 1 MHz. The electrons are generated by a 187 MHz cw gun followed by a 1.3 GHz booster and a laser heater. The first linac section (L1) accelerates the beam from 100 MeV to 250 MeV. The longitudinal phase space is linearized by two 3.9 GHz cavities prior to the first bunch compressor. After a second linac section (L2) the beam reaches the second bunch compressor at 1.6 GeV. The last linac section (L3) accelerates the beam to its final energy. Through a dogleg the beam now enters a 2 km bypass line made of stainless steel. The following kicker system distributes the individual bunches either into a tune-up dump or the two undulator transfer lines. Each undulator line is limited to 120 kW electron beam power. The power reserve in the linac allows for future undulator line additions and keep alive operation. The normal conducting 120 Hz LCLS linac is feed into the hard X-Ray line to extend the reachable photon energy range. The transfer line is separated from the linacs by a 17 m shielding wall made of iron. The movable undulator gaps produce photons in the range of 0.2 – 5 keV for LCLS-II and 1 – 25 keV for LCLS. Figure 1 shows a schematic overview of the setup.

MOTIVATION

The halo collimation system is an integral part of the LCLS-II design. We have on one hand the photo-beam of a power of up to 1.2 MW within the linac and 120 kW after the kicker system. On the other hand we can have dark current originating from cavities (including the RF gun) with a repetition rate of up to 1 MHz in the entire machine.

The most radiation sensitive part of the machine are the permanent magnets of the undulators, which should not be demagnetized above 0.01% in order to preserve FEL specifications. Current capabilities allow retuning one module per month, which means that each module should survive a minimum period of 10 years prior to re-tunning. Several irradiation experiments have been carried out to determine how much radiation the permanent magnets can tolerate to meet this specification. Measurements at SLAC End Station-A for LCLS magnets and beam energy (13 GeV), and according FLUKA [2] simulations suggested such threshold could be attained by either a high-energy fluence of 1×10^{11} n/cm^2, or a hadronic dose of 20 Gy, or a total absorbed dose of 2500 Gy. As for the last limit, a lower value of 700 Gy was finally used, based on [3] studies. Using these limits, and based on fluence and absorbed dose data generated through FLUKA simulations for 4 GeV electrons uniformly lost along the undulator beam-line with 1 and 0.1 mrad vertical deflection (up or down), it was inferred that beam losses should not exceed 12 mW/m. This corresponds to 75 lost electrons at maximal repetition rate and nominal energy.

it should be 12 mW/undulator, but even this number is too high according to my simulations. 700 Gy in 10 years will be integrated in the front magnets of each undulator for uniform losses as long as 0.6 microW/m, i.e. 0.6 mW/undulator. If we average over all magnets within a segment (which is what Jim sees relevant), then beam loss can go up by an order of magnitude, i.e. 6 mW/undulator

BEAM COLLIMATOR

The collimation system is an integral part for a high average power machine. Collimators ensure the downstream stay-clear of the accelerator. The beam stay-clear area is derived from both the betatronic and the energy stay-clear, as defined in [4].

All LCLS-II collimators are based on the same design. Each collimator consists of two independently movable uncoated rectangular jaws with circular tapering. This design allows for individual collimation in each transverse plane. To assure sufficient attenuation of dark current the jaws have a minimal thickness of 15 X_0 (6 cm). Experience from LCLS has shown a smaller collimator thickness to be insufficient [5]. Tungsten has been chosen as the material of the jaws, as it requires less real state, it can sustain higher temperatures in case of full beam strikes, and simulation for generic beams showed it has low cleaning inefficiencies. The Tungsten jaws have a minimal separation of 1 mm and can over-travel the center by 3 mm. Water-cooling allows a continuous absorption of up to 1 kW beam power per collimator jaw, and based on average beam losses and position of the collimators, shielding is installed to minimize air activation, radiation to other components, residual activity during tunnel access and radioisotope production in the groundwater surrounding the Linac. To ensure fast protection of

* marcg@slac.stanford.edu

ISBN 978-3-95450-147-2

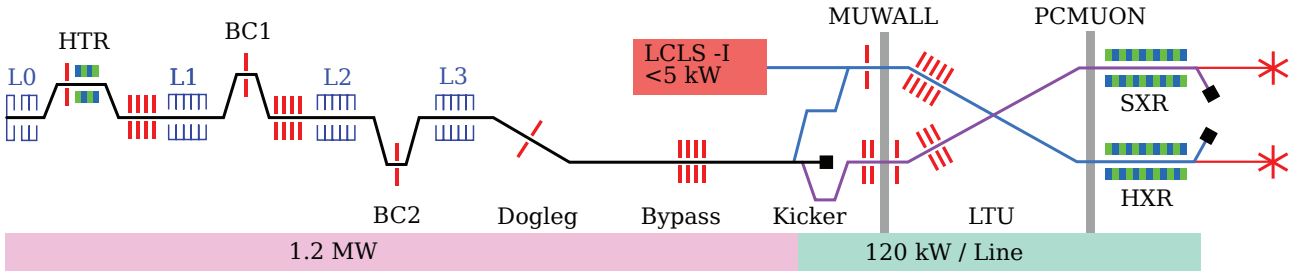

Figure 1: Schematic overview showing the superconducting LCLS-II. Whereas Cavities (blue) and collimator (red) locations are highlighted. The beam from the main linac is split into two undulator transfer lines (LTU) each serving one undulator line. In addition the normal conducting linac LCLS is feed to the hard X-Ray undulator. The undulator hall is separated from the linacs by the MUWALL (17 m iron) and PCMUON (1.5 m iron) shielding walls to reduce secondary radiation.

collimators and other devices for instantaneous full beam losses, as well as low activation of components and of the environment, ion chambers will shut off the beam at different radiation thresholds, depending on available beam power as measured by average current monitors. The fastest shut-off will happen at 100 µs, as determined through Finite Element Analysis calculations for different beam strikes on various materials.

The dark current originating from the electron gun is collimated in all 6 Dimensions before entering the undulator. Temporal collimation is performed by the beam kicker [6] (Figure 1). Transverse halo collimation is done in four FODOs. Two collimators are located at the peak β of each FODO separated by 90° phase advance, except in the undulator transfer lines. In the first three FODOs, space is reserved for an additional deferred collimator at 45° phase advance. Transverse collimation growths in importance downstream the machine as the beam halo increases due to gas-scattering. The wider bandwidth and energy separation of the dark current from the photo beam makes energy collimation very effective. The last collimator has no direct line of sight to the undulator, such that secondary radiation (gammas and neutrons) produced on the collimator jaws can not pass fixed gap collimator (1.2 m solid stainless steel) intended to shield the undulator hall from secondary radiation.

GUN DARK CURRENT

Most momenta of the dark current particles originating from gun and acceleration cavities are very different from the momentum of the photo beam. The longitudinal dark current distribution has a strong low momentum tail and a time shifted peak as compared to the photo beam. The lower momentum of the dark current with respect to the photo beam leads to a temporal delay within the laser heater and the first bunch compressor. The following linac accelerates the photo beam off-crest to generate the needed energy chirp for bunch compression. The dark current therefore gains more momentum than the photo beam and has now a higher energy peak than the photo beam, thereby slipping forward in time with respect to the photo beam. The following third linac operates at the timing insensitive on-crest. Longitudinal wakefields from cavities and the 2 km bypass line affect the photo beam stronger than the lower charge dark current, therefore further increasing the relative energy difference between them. This separation, together with the sharp decline of the photo beam on the high energy side, facilitates the collimation. The transverse dark current distribution is both bigger and has longer tails than the photo beam. It is important to collimate those tails early to prevent a significant fraction of the dark current showering unprotected magnets and electronics.

The dark current was simulated by Astra [7] to estimate the dark current distribution originating from the gun, which is then transported to the end of the first cryo module. From there on Elegant [8] simulated the beam transport up until the end of the undulator. Three different assumptions and injector configurations have been studied to increase reliability of the assessment. The simulation parameters are summarized in Table 1. This study assumes the maximal estimated dark current from the gun (400 nA [9] after the first cryo module CM01) based on the worst case measurement. Recent improvements in cathode preparations made it possible to reduce the gun dark current below 1 nA [10]. Therefore the expected cathode originated losses will likely be much lower in the actual machine.

Table 1: Simulation parameters used to create the initial beam. Note that the cathode has a diameter of 12 mm, therefore dark current originating from its entire area has been mapped.

	Photo Beam	Dark Current
Trans. Profile	Uniform	Uniform
Trans. Pulse Diameter	1.28 mm	12 mm
Long. Profile	Flat-Top	Gaussian
Long. Pulse Parameter	56 ps, rise/fall 2 ps	310 ps rms
Charge	300 pC	–
Power at CM01(100 MeV)	30 kW	40 W

The simulations reveal that the losses on all individual collimators are less than 20 W. The losses on individual magnets are below 1 W and there are no losses in the undulator section (Figure 2). Therefore, these losses do not cause machine damage. The horizontal transverse beam size of both the photo beam and the dark current are smaller than the stay-clear area throughout the machine and only 5% of the initial dark current is still present after the first bunch compressor, indicating effective collimation.

FILLED PHASE-SPACE TRACKING

To ensure the collimator effectiveness, two variants of filled phase-space tracking, with Elegant, were performed

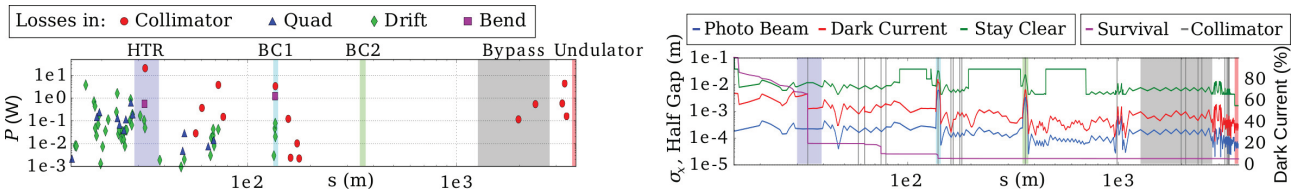

Figure 2: The right graph shows the losses of gun dark current along the machine in a log-log scale. There are no losses in the undulator section (red shaded). The left graph shows the stay-clear area (green curve), the rms horizontal transverse beam size of both the photo beam (blue) and the dark current (red) as well as the relative survival rate of the dark current (black, right scale) and the collimator location (grey shaded). The vertical plane, not presented here, shows a behavior similar to the horizontal.

as independent, self-contained study. In the first approach the entire relevant phase space was filled, 2 dimensions at a time, at the end of the linac and then tracked to the undulator exit. The lost particles are mapped to their initial distribution and binned according to their loss position. This allows to define the possible reachable places originating from any given point within the machine.

The top of Figure 3 shows the initial distribution at the exit of L3 (Figure 1) in normalized coordinates. The particles are colored according to their individual loss location. The plots show that the collimators get tighter going downstream, thereby collimating more of the initial phase space. Furthermore, they prove that there are no losses within the undulator from particles that have not been disturbed after the linac. This is strengthened by the fact that no particles after the dogleg (Figure 1) can hit the undulator.

For the alternative second variant of filled phase-space tracking we filled the relevant phase space, again 2 dimensions at a time, at the undulator entrance. The particles are then backtracked up until the exit of the linac. This simulation defines possible origin of places present at any point in the machine.

The bottom of Figure 3 shows the initial distribution binned by loss location. In agreement with the classical filled phase-space tracking, this shows that the undulator transfer line is most restrictive with the exception of a small part in the phase space which is able to travel up to the switch-yard (colored as "bypass line"). Furthermore the plots present that no uncollimated particles are outside of the ±1.5 mm undulator stay-clear (physical stay-clear within the undulator is 2.5 mm in y and 4 mm in x).

In summary, the forward tracking proved that no particle, independent of its phase space position at the beginning of the LTU, can hit the undulator. The backward tracking on the other hand proved that particles lost in the undulator do not exist at the beginning of the LTU. Combining those two findings we can therefore exclude losses due to: gun based dark current, cavity field emissions in the linac, beam halo by the beam kicker, dark current influenced through the beam kicker rise/fall and gas scattering prior to the undulator transfer line. Note that perturbations to the beam (for example through gas scattering) after this point could still lead to beam loss in the undulator.

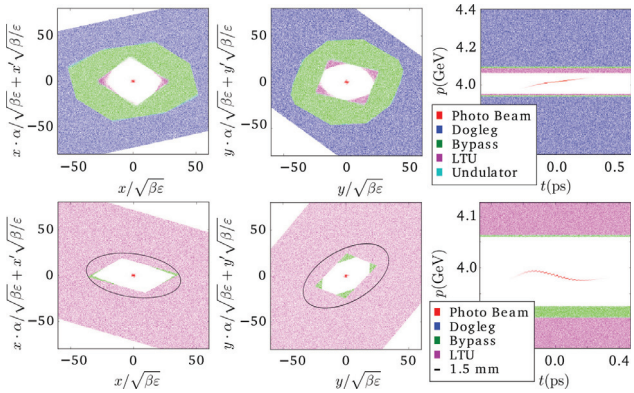

Figure 3: Top: Initial filled normalized phase space at the exit of L3 where particles have been binned according to loss section in forward tracking. Note that there are no losses within the undulator (cyan). The photo beam (red) is included for comparison. Bottom: Filled initial phase space at the undulator entrance with color binning according to loss sector in back tracking. The black ellipse corresponds to the ±1.5 mm stay-clear within the undulator.

CONCLUSION

This paper summarizes the efforts to assess the collimation system of the high power FEL LCLS-II. Special focus was placed on the undulator region where acceptable losses are as low as 12 mW (10^{-7} of the maximum photo beam power at this location). The results show that the collimation system is able to protect the machine from dark current even without exploiting its full potential.

Three different injector configurations and dark current distributions derived using different assumptions have been tracked. For all configurations, the dark current losses are under control. Filled phase space tracking has verified that no particles emerging prior to the kicker can violate the stay-clear of the undulator when transported through linear optics. This independent method further underlines the effectiveness of the collimation system.

ACKNOWLEDGMENT

The authors thank Tor Raubenheimer for fruitful discussions. This work has been supported by DOE contract #DE-AC02-76SF00515.

REFERENCES

[1] LINAC Coherent Light Source II (LCLS-II). Final design report. Technical report, SLAC, 2015.

ISBN 978-3-95450-147-2

[2] TT Böhlen, F Cerutti, MPW Chin, A Fassò, A Ferrari, PG Ortega, A Mairani, PR Sala, G Smirnov, and V Vlachoudis. The FLUKA code: developments and challenges for high energy and medical applications. *Nuclear Data Sheets*, 120:211–214, 2014.

[3] Holger Schlarb. *Collimation System for the VUV Free-Electron Laser at the TESLA Test Facility*. PhD thesis, University of Hamburg, 2001.

[4] P. Emma. Beam stay-clear aperture. Technical report, LCLSII-2.1-PR-0352, 2015.

[5] S. Mao Y. Levashov M. Santana J.N. Welch Z. Wolf H.-D. Nuhn, C. Field. Undulator RADiation damage experience at LCLS. In FEL Proceedings, editor, *Proc. 36 th Int. Free-Electron Laser Conf.*, BASEL, 2014.

[6] Tor Raubenheimer. Beam spreader. Technical report, LCLSII-2.4-PR-0090, 2015.

[7] Klaus Flöttmann. Manual: `http://www.desy.de/~mpyflo/Astra_manual/`.

[8] M. Borland. Elegant: A flexible SDDS-compliant code for accelerator simulation. Technical report, Argonne National Lab., IL (US), 2000.

[9] D. Dowell A. Fry R.K. Li Z. Li T. Raubenheimer T. Vecchione F. Zhou A. Bartnik I. Bazarov B. Dunham C. Gulliford C. Mayes A. Lunin N. Solyak J.F. Schmerge, A. Brachmann and R. Huang C. Papadopoulos G. Portmann J. Qiang F. Sannibale S. Virostek R. Wells A. Vivoli, D. Filippetto. The LCLS-II injector design. In FEL Proceedings, editor, *Proc. 36 th Int. Free-Electron Laser Conf.*, BASEL, 2014.

[10] John Schmerge. Injector and laser systems. FAC Review, Feb 2015.